An Improved Feature Extraction Method for Texture Classification with Increased Noise Robustness

Stefania Ramona Barburiceanu
Communications Department,
Technical University of Cluj-Napoca
Cluj-Napoca, Romania
Stefania.Barburiceanu@com.utcluj.ro

Serban Meza
Communications Department,
Technical University of Cluj-Napoca
Cluj-Napoca, Romania
Serban.Meza@com.utcluj.ro

Christian Germain
Laboratoire de l'Intégration du
Matériau au Système
Université de Bordeaux,
Talence, France
christian.germain@ims-bordeaux

Romulus Terebes
Communications Department,
Technical University of Cluj-Napoca
Cluj-Napoca, Romania
Romulus.Terebes@com.utcluj.ro

***Abstract*—This paper presents an improved feature extraction method based on the use of state-of-the art filtering techniques and Local Binary Patterns-derived feature descriptors with applications in texture classification. The method is adaptive, being capable to determine the type of noise present in the input image and to apply the appropriate operator for the filtering step of the feature extraction technique. The improved approaches, labelled BM3DELBP (Block Matching and 3D filtering Extended Local Binary Pattern) and SARBM3DELBP (Synthetic Aperture Radar Block Matching and 3D filtering Extended Local Binary Pattern) bring significant improvements both in terms of robustness to Gaussian and speckle noise and in terms of classification accuracy, being invariant to different image transformations. We tested our approach both on synthetic textures from two standard Outex databases and on real polarimetric Synthetic Aperture Radar (SAR) images of pine forests. On all considered databases, the proposed approach proved to be above state-of-the-art LBP variants in terms of classification accuracy, even in the presence of high Gaussian and speckle noise levels.**

Keywords— texture classification, Local Binary Patterns, Block Matching, 3D filtering, noise robustness, feature extraction, SAR images, speckle noise, Gaussian noise

I. INTRODUCTION

Texture classification is a very important technique used in several domains such as medical imaging, remote sensing or industrial inspection. Supervised texture classification consists in assigning an unknown texture to one of the predefined texture classes and regardless of the application, always includes two steps: the learning step in which a model is generated based on the textural content and the classification step in which the category is predicted for a new sample based on the created model. Two important techniques are used for supervised image classification: feature extraction and machine learning classification. Feature extraction involves generating characteristics from raw data that are relevant and discriminative. The performance of the system strongly depends on the set of extracted characteristics, the goal being to provide a reduced representation that will maximize the classification accuracy with as little data as possible. The classification of real-world textures is a difficult process due to variable conditions at which images are exposed, so for achieving a reliable classification, the extracted entities must be invariant to different transformations in the input, for example rotation, change of the observation scale, illumination and must also be robust to noise. One of the most popular methods used to extract features is represented by the original LBP (Local Binary Pattern) operator, introduced by the seminal work of Ojala [1]. Researchers gave importance to this feature extraction method because of its invariance to monotonic grey-scale changes caused, for example, by variations of illumination, its simplicity and speed of computation. However, the original LBP operator is not capable to capture large scale structures and is not invariant to rotation and scale of observation. That is why in [2], the same authors extended the original formulation by using neighbourhoods of variable sizes, the uniform patterns criterion and the multiresolution approach. Many other variants of LBP have been developed recently to create new, more discriminative and robust operators. They include the Completed Local Binary Pattern (CLBP) operator [3], the Extended Local Binary Pattern (ELBP) [4] and the Discriminative Completed Local Binary Pattern operator (disCLBP) [5]. All these variants were proposed to improve the discrimination power, but they were still very sensitive to noise. For handling also noise, other variants of LBP have been proposed: Local Ternary Patterns (LTP) [6], Noise Resistant Local Binary Patterns (NRLBP) [7], Median Binary Patterns (MBP) [8] and Median Robust Extended Local Binary Patterns (MRELBP) [9].

Nowadays there are several efficient noise removal techniques, their performances depending strongly on the noise nature. In this context, noise type identification methods have been developed. Approaches based on local histograms [10] perform noisy image segmentation using a multi-thresholding technique followed by a noise identification criterion on selected homogeneous regions. In [11], the noise identification is performed with the help of neural networks. Another method is the one proposed in [12], where identification is performed by extracting statistical features on which a simple pattern classification approach operates.

We propose a novel feature extraction method that accurately detects the noise type present in the input images and applies the appropriate filtering in the feature extraction process. The new operators, BM3DELBP and SARBM3DELBP, generate characteristics with good invariance properties with respect to the change of the observation scale, to different lighting conditions and to

978-9-0827-9703-9/19/$31.00 ©2019 IEEE

rotation, having also increased robustness to Gaussian and speckle noise. Our method builds on the MRELBP approach [9], which inherits the illumination change invariance of the original LBP version. Moreover, it is rotation invariant since it relies on an invariant coding scheme. Due to the multiresolution approach, it has also a degree of invariance to the change of the observation scale. Although being described to offer an excellent noise robustness when compared to other state of the art LBP variants, this is true only for low noise levels (the higher Gaussian noise standard deviation used for tests in [9] was $\sigma = 5$). However, for higher noise levels, the performance of the MRELBP operator drops drastically and thus, the noise robustness is unsatisfactory. We were therefore interested in building operators more robust at higher noise levels, for both Gaussian and speckle noise situations.

II. Related Work

A. Local Binary Patterns

The original LBP operator [1] works locally on grayscale images by computing an LBP code at each pixel location, considering a small neighbourhood, centred at x_c. Each pixel is compared to its $P = 8$ neighbours and the resulting 8-bit binary number is then converted to decimal. This process is repeated for each pixel of the input image and finally, a histogram accounting for the obtained LBP codes is built. In order to capture texture characteristics at different scales, the original LBP formulation was extended to use neighbourhoods of different sizes [2]. It has also been indicated that the greater the number of spatial transitions in the pattern, the more likely it is that the pattern will change to a different pattern during rotation. Based on this argument, the authors in [2] introduce the notion of uniform patterns, these patterns being those which have at most two bit-wise transitions, so that the value of U (uniformity function) is at most equal to 2. Moreover, in order to gain rotation invariance, the uniform patterns are grouped in P+1 categories which are rotation invariant. It results the $LBP^{riu2}_{R,P}$ given in (1), which generates P+2 histogram bins.

$$\mathrm{LBP}^{\mathrm{riu2}}_{\mathrm{R,P}}=\begin{cases}\sum_{k=0}^{P-1} s(x_c - x_{R,P,k}), \text{ if } U(\mathrm{LBP}_{R,P})\leq 2\\ P+1, \text{ otherwise}\end{cases} \quad (1)$$

x_c is the central pixel, $s(x)$ is the sign function, $x_{R,P,k}$ is the k^{th} neighbour in a neighbourhood of radius R and P neighbours and the superscript *riu2* reflects the use of uniform rotation invariant patterns that have a U value at most equal to 2.

B. Median Robust Extended Local Binary Patterns

In the MRELBP approach, for building the feature space, three components are calculated: *MRELBP_CI* (Central pixel's Intensity),*MRELBP_NI* (Neighbours' Intensities) and *MRELBP_RD* (Radial Difference). Their expressions are given in (2), (3) and (5), as defined in [9].

$$\mathrm{MRELBP\_CI}(x_c)=s(\varphi(X_{c,w})-\mu_w)) \quad (2)$$

$X_{c,w}$ designates the local patch of size $w \times w$ centred on the central pixel x_c, $\varphi(X)$ is the median value of X and μ_w is the average of $\varphi(X_{c,w})$ over the entire image.

$$\mathrm{MRELBP\_NI}_{R,P}(x_c)=\sum_{n=0}^{P-1} s(\varphi(X_{R,P,w_R,n})-\mu_{R,P,w_R})) \times 2^n \quad (3)$$

μ_{R,P,w_R} is defined in (4) and $X_{R,P,w_R,n}$ designates the patch of size $w_R \times w_R$ centred on the neighbouring pixel $x_{R,P,n}$.

$$\mu_{R,P,w_R}=\frac{1}{P}\times\sum_{n=0}^{P-1}\varphi(X_{R,P,w_R,n}) \quad (4)$$

$$\mathrm{MRELBP\_RD}(x_c)=\sum_{n=0}^{P-1} s(\varphi(X_{R,P,w_R,n})-\varphi(X_{R-1,P,w_{R-1},n}))\times 2^n \quad (5)$$

MRELBP_RD is based on the differences of pixels' intensities on two circles centred on the central pixel and having the radii R and $R-1$.

C. Block Matching and 3D filtering and SAR Block Matching and 3D filtering

The Block Matching and 3D filtering (BM3D) [13] is considered the state-of-the-art for image denoising and surpasses all other methods for filtering out Gaussian noise. This method is based on a reinforced sparsity in the transform domain, which is done by grouping 2D blocks in 3D groups, such that they are similar to a reference block whose structure is better estimated in this way. 3D denoising is performed using a collaborative filtering approach that performs a 3D transform in which the signal is sparsely represented. The noise is eliminated by a shrinking operation on the transform coefficients. The BM3D filter was also adapted in [14] to deal with speckle noise, yielding to SAR-BM3D. The same filtering structure as in the BM3D filter is used, considering some modifications: the replacement of the Euclidean distance with an optimized block similarity measure when collecting blocks in 3D groups and the collaborative filtering type, adopting the Linear Least Mean Squared Error solution.

III. Proposed Method

The RELBP (Robust Extended LBP) operator [9] embeds a filtering operation performed prior to the feature extraction part. The authors study three possible solutions for this step, mean, median and Gaussian smoothing filters, without proposing an algorithm for adaptively switching between them. Based on an extensive experimental evaluation, the authors opt to use the median since it possesses a nonlinear robust behaviour, the resulting operator being called MRELBP. We developed an improved feature extraction method that includes a noise identification step, a filtering technique and a feature extraction descriptor. Its flowchart is given in Fig. 1. The noise identification is used to choose adaptively the filtering technique according to the identified type of noise. The last step, the feature extraction descriptor, is used to generate characteristics with good invariance properties with respect to lighting conditions, observation scale, rotation and noise.

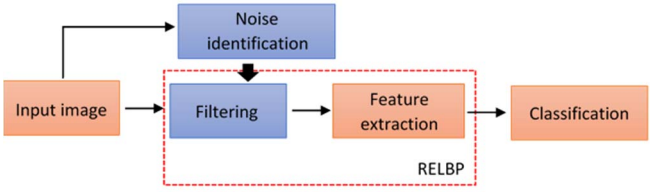

Fig. 1. The flowchart of our approach

A. Improved feature extraction method

With respect to Fig.1, our improved method preserves the feature extraction descriptor of *RELBP* and the idea of a filtering technique, but replaces the median filter used in [9]. The approach encloses a supplementary step, the noise type identification, adaptively switching between the proposed

operators, BM3DELBP and SARBM3DELBP. The robustness to noise is increased by applying these state-of-the-art filters in the feature extraction technique.

1) Noise identification step

This step relies on the work in [12] and considers the same noise types: Gaussian, speckle and salt and pepper. However, unlike in [12], the training and test phases were designed differently in our approach, as shown in Fig. 2. In the training phase, only images from the training set were considered (the same set was used in the subsequent feature extraction and texture classification processes). The three types of noise were added to the images of this set, forming a three times bigger noisy training set. Each training image was filtered by the three different filtering techniques, the filtered versions being then subtracted from the noisy input images in order to obtain three noise estimates. For each noise estimate, we computed two statistical features, kurtosis and skewness, finally obtaining a feature vector containing six characteristics. For the test phase, we used only the images from the test set (the same one used in the classification process), each image being affected by an unknown noise type. The same process for feature extraction was followed in order to obtain the test feature vector. Unlike [12], we used all characteristics for all training samples, not just a reference value. By taking only the mean value of the statistical features from all training samples, important information is lost. Since there are multiple texture classes involved, the mean value was not sufficient to describe one type of noise. Finally, the SVM (Support Vector Machine) classifier (chosen as it provided the best results) with polynomial kernel was used to identify the noise type present in the images.

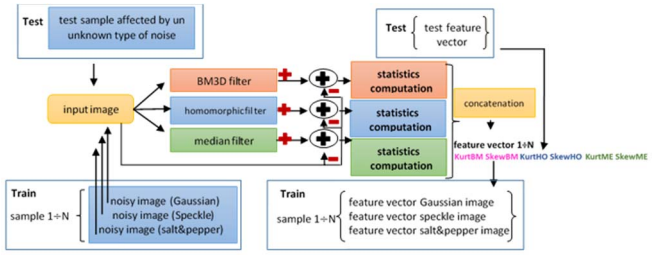

Fig. 2. Noise type identification flowchart

2) The BM3DELBP and SARBM3DELBP operators

The proposed descriptor, BM3DELBP, was designed to be more robust to noise than MRELBP, even for high Gaussian noise levels. To this aim, we propose the replacement of the median filter with the BM3D one [13]. Fig. 3 shows the block schema used to build the BM3DELBP descriptor. Practically, a noisy texture was used as input for the system, and then the BM3D filter was applied. After filtering the image, for each scale of interest (2, 4, 6 and 8), three operators were extracted: *BM3DELBP_CI*, $BM3DELBP\_NI^{riu2}_{R,P}$ and $BMM3DELBP\_RD^{riu2}_{R,P}$. The first operator was calculated exactly as in (6), *BM3DELBP_NI* and *BM3DELBP_RD* defined in (7) and (9) produce 2^P different binary models. To remove the rotation effect and to reduce the size, the rotation invariant and uniform mapping (*riu2*) was applied.

$$BM3DELBP\_CI=s(x_c-C_I) \quad (6)$$

with C_I the mean of the entire image

$$BM3DELBP\_NI=\sum_{n=0}^{P-1} s(x_{R,P,n}-u_R)\times 2^n \quad (7)$$

$$u_R=\frac{1}{P}\times\sum_{n=0}^{P-1} x_{R,P,n} \quad (8)$$

$$BMM3DELBP\_RD=\sum_{n=0}^{P-1} s(x_{R,P,n}-x_{R-1,P,n})\times 2^n \quad (9)$$

For each scale, the codes obtained by using the three operators were combined using a three-dimensional joint histogram. The code *BM3DELBP_NI* has 2 values (0 and 1), $BM3DELBP\_NI^{riu2}_{R,P}$ and $BMM3DELBP\_RD^{riu2}_{R,P}$ each have $P+2$ values and thus, a joint histogram has $(P+2)\times(P+2)\times 2$ values. After obtaining a joint histogram for each scale, all joint histograms from all scales were concatenated and formed the final histogram which was used as texture descriptor.

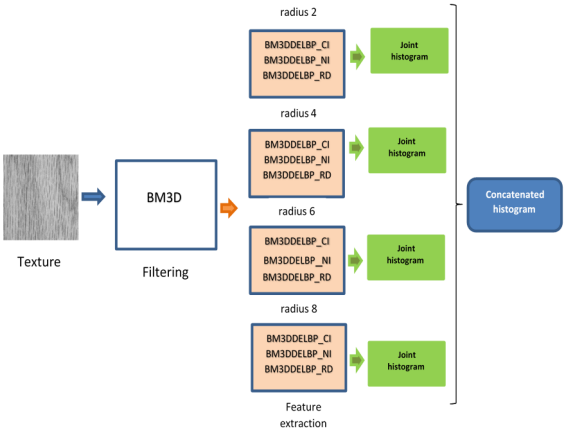

Fig. 3. The BM3DELBP operator functional diagram

The SARBM3DELBP operator is constructed in the same manner as BM3DELBP, the only difference being the filter used, which is in this case the SAR-BM3D filter [14].

B. Classification algorithms

For the classification phase of our approach, we used the kNN (k-Nearest Neighbours) and the SVM classifiers. The kNN algorithm operating with the chi squared ($\chi 2$) distance (specifically designed for comparing histograms) [15] was used for the synthetic textures case in order to maintain the consistency with the results given in [9]. The SVM classifier (with polynomial kernels [16]) was chosen by trial and error for real polarimetric images as it provided the best results.

IV. Experimental Results

A. Databases

1) Synthetic texture databases

The first database used in our experiments is Outex_TC_00012 [17], which contains 24 texture classes from a wide variety of real-world materials and is considered a difficult test suite for rotation and illumination invariant classification. In our experimental configuration, we used images captured under 2 different illuminations: "inca" and "tl84". In the case of "tl84", for each class, we used 20 different samples for each of the 9 orientation angles (0º, 5º, 10º, 15º, 30º, 45º, 60º, 75º and 90º). In the case of the "inca" illuminant, 20 samples were considered for each class only for the 0º angle. Out of the total of 4800 samples, we used 70% for training and 30% for testing and 40 random partitions of the learning and test sets were used to report the results. The second database used in the experiments is the Outex_TC_00013 database [17]. It contains 68 classes and unlike the first database, all textures were captured under

"inca" lighting condition and 0º orientation angle. There are 20 non-overlapping samples for each texture class, giving a total number of 1360 samples that were used to test the texture classification methods by using 40 random partitions.

2) The PolSAR images database

This database was used to test the behaviour of the proposed method for Polarimetric SAR image classification. It contains patches collected from an image which represents a forest of maritime pines from France, similar images being also encountered in precision agriculture applications. Fig. 4 shows the polarimetric image used in our experiment which contains 62 forest patches grouped into 4 classes according to their age [18]: between 5 and 7 years old, 12 and 15, 21 and 29 and 32 and 48 years old. The mask overlaid on the image shows the parcels used in the classification task, being marked with different colours according to their age indicated in the legend on the image left side. Ground truth data is available only for the mask. We used 70% of samples (43) for training disposed as follows: 5-7 years: 7 samples, 12-15 years: 3 samples, 21-29 years: 29 samples, 32-48 years: 4 samples and 30% (19) for testing: 5-7 years: 3 samples, 12-15 years: 2 samples, 21-29 years: 12 samples, 32-48 years: 2 samples and 60 random partitions were formed to obtain the results.

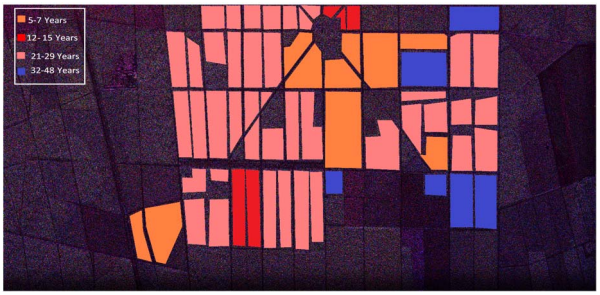

Fig. 4. The parcels used from the PolSAR image [18]

B. Results

We performed noise type identification and then we tested the noise robustness and the classification accuracy of our method, in comparison to MRELBP. For the classification step, both kNN and SVM classifiers were used, but we report here only the best results. In order to test the robustness to noise of the feature extraction operators, we used for the Outex databases noise free images for the training step and images affected by noise (zero-mean Gaussian noise and speckle noise generated using (10)) for the test phase. For the real PolSAR image database, we had only the noisy patches, so we used them for both phases. We performed filtering only for noisy images (except for the noise free test where we used BM3DELBP for both sets) in our approach, while for MRELBP, filtering was done for noise free and noisy images in all cases as proposed in [9].

$$J = I + n \times I \qquad (10),$$

where n is uniformly distributed random noise with mean 0 and variance Var, J is the noisy image and I the noise free one.

The parameters used for the proposed operators are: the noise standard deviation for BM3D (corresponding to the intensities in the range [0,255]) which we denoted m and the number of looks of the speckle noise for SAR-BM3D, denoted L. For all databases, the following parameters were used: w=3, P = 8, 4 different radii R (2, 4, 6 and 8) and w_r= R + 1. Parameters m and L were tuned in order to obtain the highest accuracy scores. In practice, L is known or it can be estimated. As far as m is concerned, this is an intrinsic parameter of the BM3D method and is correlated with the standard deviation of the noise. In our approach we let m vary as we chose it as a trade-off between attenuation of noise and texture removal.

1) OUTEX_TC_00012 database results

For images affected by Gaussian noise, the optimal values for m are 21 for high noise levels and 4 for low noise levels, both for noise type identification and classification. The best results for the speckle noise case were obtained for L=6. The noise type identification accuracy is given in Table I. As it shows, the noise identification figures are very high. Feature extraction and texture classification were subsequently performed. We show the obtained results in Table II.

TABLE I. NOISE TYPE IDENTIFICATION ACCURACY [%] OUTEX_12

Gaussian noise σ = 5	***Gaussian noise σ = 25***	***Speckle noise Var=0.04***	***Salt&pepper 2%***
99.99±0.03	99.99±0.03	99.97±0.03	100±0

TABLE II. CLASSIFICATION ACCURACY [%] OUTEX_12

Noise type	**kNN 3 neighbours and χ2 distance**	
	MRELBP	***BM3DELBP/ SARBM3DELBP***
NOISE FREE	**99.99±0.02**	99.87±0.09
GAUSSIAN σ = 5	94.87±0.18	**99.8±0.12**
GAUSSIAN σ = 25	45.45±1.48	**91.35±0.68**
SPECKLE Var=0.04	21.85±0.70	**86.72±0.5**

Table II shows a good classification accuracy for the MRELBP operator [9] in the absence of noise and for a low-level Gaussian noise. However, its performance dropped considerably for a high-level Gaussian noise, which proves that its robustness to noise is unsatisfactory, being also surpassed by the ARELBP (Average RELBP) operator which achieved 61.37%±0.75. On the other hand, our proposed operator, BM3DELBP, proved to be also robust at high Gaussian noise levels, giving higher figures both than MRELBP and ARELBP. The results are remarkable since all training images were noise free. In case of the speckle noise, MRELBP achieved a very low classification accuracy even if the level of noise was not high, but SARBM3DELBP gave a high classification accuracy.

2) OUTEX_TC_00013 database results

For the noise identification step, the optimal value for m in the medium noise level case is 10 and 21 in the high level case. For the classification step, for the high noise level, we obtained the best classification accuracy for m=15 and L=11 and for the medium one, for m=5 and L=13. The noise type identification step accuracy is given in Table III.

TABLE III. NOISE TYPE IDENTIFICATION ACCURACY [%] OUTEX_13

Gaussian σ = 10	***Gaussian σ = 25***	***Speckle Var=0.02***	***Speckle Var=0.04***	***Salt and pepper 2%***
99.07±0.56	99.12±0.39	99.36±0.38	99.56±0.30	99.78±0.35

The results from Table III reveal that also for this database, the noise type identification approach is successful, giving high accuracy figures. Based on these results, we obtained in the texture classification step the accuracy figures in Table IV.

The results lead to the conclusion that classification accuracy for noise free images in the MRELBP case is worse comparing to the first database and its performance drops significantly even for a medium level of Gaussian noise. For high Gaussian noise levels, its performance is drastically decreased. However, the classification performance is considerably improved by using the BM3DELBP operator. For images affected by speckle noise, the MRELBP operator performed also poorly even on low noise levels, while the SARBM3DELBP operator greatly improved the performance. As expected, in case of the salt and pepper noise, the MRELBP operator performed better than the proposed operators, the median filter being adapted to this type of noise. Thus, our system can be generalized to use median filtering for images affected by salt and pepper noise, as for MRELBP.

TABLE IV. CLASSIFICATION ACCURACY [%] OUTEX_13

	kNN 5 neighbours and $\chi 2$ distance	
Operator/noise type	***MRELBP***	***BM3DELBP/SARBM3ELBP***
NOISE FREE	82.03±0.8	**82.82±1.2**
GAUSSIAN σ = 10	45.8±1.72	**69.31±1.72**
GAUSSIAN σ = 25	15.83±0.88	**42.11±1.52**
SPECKLE Var=0.02	26.37±0.75	**58.63±2**
SALT&PEPPER 2%	**81.42±1.58**	32.43±0.95/20.96±0.8

3) PolSAR image database results

We also tested our feature extraction method on a real PolSAR image in order to classify the forests 'patches according to their age. Being a fully-polarimetric image, we analysed all polarimetric channels, but only report here the results for the HH channel, giving the best performance. We analysed the noise robustness of the SARBM3DELBP operator. The obtained results are given in Table V.

TABLE V. CLASSIFICATION ACCURACY [%] POLSAR IMAGES

Descriptor	**L=15 and SVM with polynomial kernel**
MRELBP	78.55±8.54
SARBM3DELBP	**85.13±8.25**

The obtained results reveal that the SARBM3DELBP operator surpasses MRELBP also on real world PolSAR images. By implying an appropriate filtering for the speckle noise, the texture structures were kept and thus the classification performance increased.

V. CONCLUSIONS AND FUTURE WORK

We proposed an adaptive feature extraction method to improve the noise robustness and the classification accuracy of LBP-based feature extraction methods. In order to achieve our goals, we derived our work from the RELBP operator which is a state-of-the-art LBP variant and we proposed the replacement of the median filter with the BM3D filter in the case of Gaussian noise and with the SAR-BM3D filter in case of the speckle noise. In addition to the change in the filtering step, we developed a very accurate noise type identification approach, which proved to identify very well the type of noise present in the input images. According to the identified type of noise, one of the two filters were used in the feature extraction process. Our proposed approach improved the classification accuracy significantly, outperforming existing LBP-based approaches in terms of Gaussian and speckle noise robustness, even for high noise levels. Further work will be devoted to the development of a feature extraction method that relies on deep convolutional neural networks, for both classic and hyperspectral images and of new filtering techniques.

ACKNOWLEDGMENT

This work was supported by a grant of the Romanian Ministry of Research and Innovation, CCCDI-UEFISCDI, project number PN-III-P1-1.2-PCCDI-2017-0251/4PCCDI/ 2018, within PNCD III.

REFERENCES

[1] T. Ojala, M. Pietikäinen and D. Harwood, "A comparative study of texture measures with classification based on feature distributions", Pattern Recognition, vol. 29, pp. 51-59, January 1996.

[2] T. Ojala, M. Pietikainen and T. Maenpaa, "Multiresolution gray-scale and rotation invariant texture classification with local binary patterns", IEEE Trans. Pattern Anal. Mach. Intell, vol. 24, pp. 971–987, July 2002.

[3] Z. Guo, L. Zhang and D. Zhang, "A completed modeling of local binary pattern operator for texture classification", IEEE Trans. Image Process., vol. 19, pp. 1657 – 1663, June 2010.

[4] L. Li, L. Zhao, Y. Long, G. Kuang and P. Fieguth, "Extended local binary patterns for texture classification", Image and Vision Computing, vol. 30, pp. 86-99, February 2012.

[5] Y. Guo, G. Zhao and M. Pietikäinen, "Discriminative features for texture description", Pattern Recognition, vol. 45, pp. 3834-3843, October 2012.

[6] X. Tan and B. Triggs, "Enhanced local texture feature sets for face recognition under difficult lighting conditions", IEEE Trans. Image Processing, vol. 19, pp. 1635 – 1650, June 2010.

[7] J. Ren, X. Jiang and J. Yuan, "Noise-resistant local binary pattern with an embedded error-correction mechanism", IEEE Trans. Image Processing, vol. 22, pp. 4049-4060, October 2013.

[8] A. Hafiane, G. Seetharaman and B. Zavidovique, "Median binary pattern for textures classification" in International Conference on Image Analysis and Recognition, 2007, pp. 387–398.

[9] L. Liu, S. Lao, P. W. Fieguth, Y. Guo, X. Wang and M. Pietikäinen, "Median Robust Extended Local Binary Pattern for Texture Classification", IEEE Trans. Image Processing, vol. 25, pp. 1368-1381, March 2016.

[10] M. Ghouse and M. Siddappa, "Adaptive techniques based high impulsive noise detection and reduction of a digital image", Journal of Theoretical and Applied Information Technology, vol. 24, pp. 41-49, February 2011.

[11] K.G. Karibasappa, S. Hiremath and K. Karibasappa, "Neural Network Based Noise Identification in Digital Images", The Association of Computer Electronics and Electrical Engineers International Journal on Network Security, vol. 2, pp. 28-31, July 2011.

[12] Y. Chen and M. Das, "An automated technique for image noise identification using a simple pattern classification approach", 2007 50th Midwest Symposium on Circuits and Systems, pp. 819-822, August 2007.

[13] K. Dabov, A. Foi, V. Katkovnik and K. Egiazarian, "Image denoising by sparse 3D transform-domain collaborative filtering", IEEE Trans. Image Process., vol. 16, pp. 2080—2095, August 2007.

[14] S. Parrilli, M. Poderico, C. V. Angelino and L. Verdoliva, "A Nonlocal SAR Image Denoising Algorithm Based on LLMMSE Wavelet Shrinkage", IEEE Transactions on Geoscience and Remote Sensing, vol. 50, no. 2, pp. 606-616, February 2012.

[15] Y. Rubner, C. Tomasi and L. J. Guibas, "The Earth Mover's Distance as a Metric for Image Retrieval", International Journal of Computer Vision, vol. 40, pp. 99-121, November 2000.

[16] Christopher J. C. Burges, "A Tutorial on Support Vector Machines for Pattern Recognition", Data Mining and Knowledge Discovery, pp. 121-167, June 1998.

[17] "Outex Texture Database", Internet: http://www.outex.oulu.fi/index.php?page=classification, [Nov. 2018].

[18] I. Ilea, "Robust classification methods on the space of covariance matrices: application to texture and polarimetric synthetic aperture radar image classification", Ph.D. dissertation, University of Bordeaux, Bordeaux, 2017.